Electronic Supplementary Material (ESI) for Polymer Chemistry.

Supplementary information

Mechanical Properties of Single Supramolecular Polymers from Correlative AFM and Fluorescence Microscopy

M.A. Beuwer[1,3], M.F. Knopper[1], L. Albertazzi[3,4], D. van der Zwaag[3,5], W.G. Ellenbroek[3,6], E.W. Meijer[3,5], M.W.J. Prins[1,2,3] and P. Zijlstra[1,3],

[1]Molecular Biosensing for Medical Diagnostics, Faculty of Applied Physics, Eindhoven University of Technology, PO Box 513, 5600 MB, Eindhoven, The Netherlands; [2]Molecular Biosensing for Medical Diagnostics, Faculty of Biomedical Engineering, Eindhoven University of Technology, PO Box 513, 5600 MB, Eindhoven, The Netherlands; [3]Institute for Complex Molecular Systems, Eindhoven University of Technology, PO Box 513, 5600 MB, Eindhoven, The Netherlands; [4]Institute for Bioengineering of Catalonia (IBEC), Carrer de Baldiri Reixac 15-21, 08028 Barcelona, Spain; [5]Laboratory of Macromolecular and Organic Chemistry, Faculty of Chemical Engineering and Chemistry, Eindhoven University of Technology, PO Box 513, 5600 MB, Eindhoven, The Netherlands; and [6]Theory of Polymers and Soft Matter, Faculty of Applied Physics, Eindhoven University of Technology, PO Box 513, 5600 MB, Eindhoven, The Netherlands.

Table of Contents

Introduction on quantifying persistence length

Inextensible polymers that exhibit a resistance to bending are usually described with the worm-like chain model.[1] The key parameter of this model is the bending stiffness κ. Describing the position along the polymer chain (length L) with a coordinate $s \in (0,L)$, measured along the polymer backbone, $\vec{r}(s)$ is the position of a chain segment and $\hat{t}(s) = d\vec{r}/ds$ is a unit tangent vector denoting the local orientation.

The key physics of the bending resistance is captured in the model by introducting an energy penalty on gradients of $\hat{t}(s)$, given by

$$E_{bend} = \frac{\kappa}{2} \int ds \left| \frac{d\hat{t}}{ds} \right|^2, \tag{S1}$$

so that higher bending moduli lead to straighter chains. The combined effect of thermal fluctuations and bending stiffness then leads to a typical length (measured along the backbone) over which the chain orientation decorrelates, the persistence length $L_p = \kappa/(k_B T)$. This length can be extracted from any form of data that describes the local orientation of the polymer chain as a function of contour length s, by fitting the tangent vector autocorrelation to its theoretical prediction:[2]

$$C(s) = \langle \hat{t}(s) \cdot \hat{t}(0) \rangle = \exp\left[-\frac{s}{2l_p} \right]. \tag{S2}$$

Here the average is taken over an ensemble of similar chains. The factor 2 in this equation is only present for chains adsorbed onto a flat surface, as we study in this paper. In adsorbed chains, the tangent vector can be represented with a single angle $\theta(s)$ indicating the angle between $\hat{t}(s)$ and a chosen reference axis in the plane of the surface, and the average can be rewritten as $C(s) = \langle \cos[\theta(s) - \theta(0)] \rangle$. We therefore refer to $C(s)$ as the *cosine correlation function*.

Persistence length analysis

In order to find the persistence length of adsorbed two-dimensional semi-flexible polymers the tangent angles at coordinates along the polymer are calculated from the polymer backbone. From these tangent angles the apparent persistence length is calculated for each polymer using cosine correlation analysis.

The polymer backbone of each polymer was obtained by pre-processing the raw image of the polymers (Fig. 1a) using the free image-processing software *ImageJ* based on a similar approach as Graham *et al.*[3] Using thresholding and skeletonization (Fig. 1d), i.e. creating a one-pixel-wide backbone by eliminating the outer pixels of the polymer, the polymer backbone can be analysed using our persistence length analysis script. However, due to pixelation the polymer backbone doesn't always follow the polymer, because the pixel size is large compared to the width of the polymer. This created curvature in the backbone that is not present in the polymer, therefore prior to thresholding images were interpolated with a factor 9, i.e. each pixel is divided into nine subpixels, where each subpixel is given a weighted intensity of its nearest neighbours (Fig. 1b). To further improve localization of the polymer backbone the polymer was deconvolved with a 2D Gaussian with the FWHM of the experimental point spread function (Fig. 1c). Before thresholding and skeletonization, the image was Gaussian-smoothed to improve thresholding. The Gaussian smoothing was necessary to smooth inhomogeneities in the intensity caused by deconvolution of a noisy image, the Gaussian kernel used was however much smaller than the 2D Gaussian used for devonvolution.

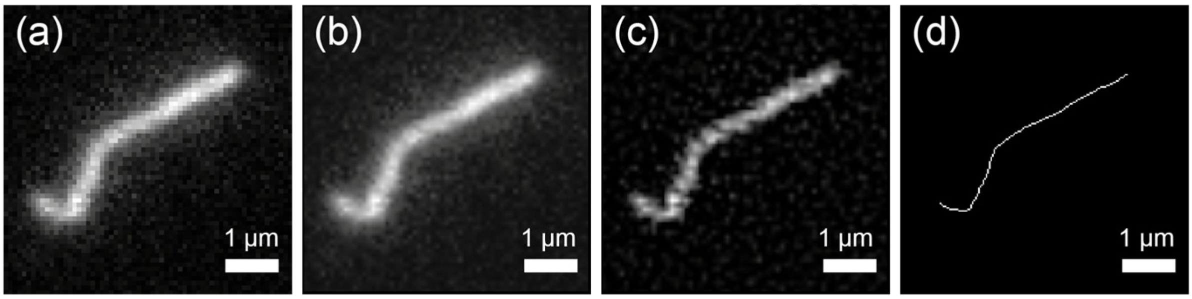

Fig. S1. Pre-processing of the raw image to extract the polymer backbone. The raw image of a polymer (a) is pre-processed by enhancing contrast and interpolation (b) to improve the shape of the final one-pixel-wide backbone. The polymer is deconvolved with a 2D Gaussian to decrease its width (c) and is finally thresholded and skeletonized, resulting in a one-pixel-wide polymer backbone (d).

The backbone coordinates are then smoothed by fitting a third-order Beziér spline using Matlab (The MathWorks Inc., Natick, MA). For each coordinate along the reconstructed polymer, the tangent angle is calculated and from these tangent angles the cosine correlation, as defined below, is calculated.

The persistence length is calculated by fitting the cosine correlation function for two-dimensional (2D) fluctuations (equation S3) to the averaged cosine correlation values. When applied to a single immobilized polymer an apparent persistence length is obtained, as the polymer is in one of infinite configurations. Only when performing cosine correlation on many configurations of one polymer or many of the same polymer the persistence length is obtained.

Simulated polymers using the worm-like chain model

In this paper, we use the term “apparent persistence length” to describe the persistence length of a single adsorbed polymer. This quantity is obtained by fitting an exponential function to the cosine correlation function usually used to describe the ensemble-average persistence of many chains with the same underlying bending stiffness κ. With the definition $L_p = \kappa/(k_B T)$, we have, for a chain adsorbed on a surface,[1]

$$C(s) = \left\langle \cos\left[\theta(s+s_0) - \theta(s_0)\right]\right\rangle_{s_0} = e^{-s/(2l_p)} . \qquad \text{(S3)}$$

Here, we average only over different starting points s_0 along the same chain, resulting in a single-chain apparent persistence length. The fitting procedure focuses on small values of s, as this procedure provides poor statistics for $s > 0.1L$.

In order to relate the distributions of these apparent persistence lengths to the underlying persistence length (intrinsic bending stiffness) of the experimental polymers, we need to know how they are influenced by noise and other experimentally unavoidable limitations to accuracy. To this end we employ a sample of computer-generated worm-like chains with an underlying (ensemble-averaged) persistence length of $L_p = 1.5\ \mu m$, and analysed them with the same procedure used to analyse the TIRF-images from our experiments.

We represent numerical worm-like chains as discrete jointed chains with straight segments of length Δs and angles between consecutive segments drawn from a normal distribution with variance $\Delta s/L_p$ (see Fig. S2). This procedure amounts to discretizing the integral in equation (S1) and applying the equipartition theorem. These angles uniquely determine the shape of the adsorbed chain. We can calculate the exact cosine correlation function of this model because it is written in terms of the same angle $\theta(s)$ that defines this correlation. Thus, we have precise values for the apparent persistence length of these chains, the distribution of which we can compare to experiments.

The sample used to generate Figure 7 in the main text consisted of 100 worm-like chains of length $10\ \mu m$, represented using 400 segments of length 25 nm (which is below the pixel size for all subsequent analyses). An example is shown in Figure S2.

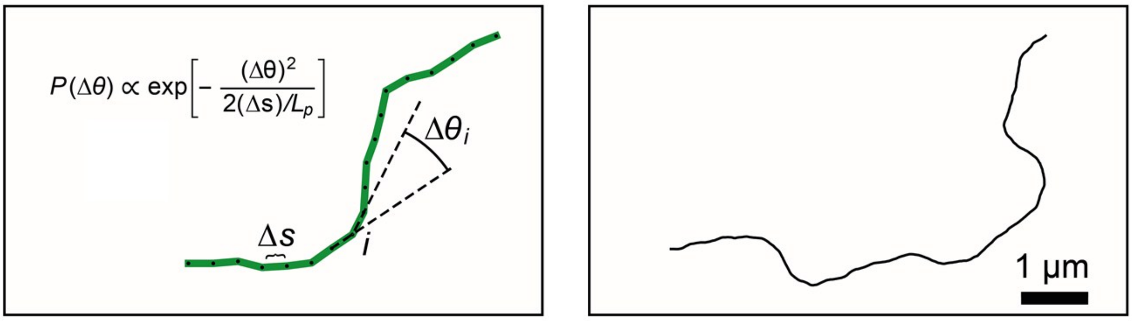

Fig. S2. Simulated polymer using the worm-like chain model. (a) Fragment of simulated polymer with $\Delta s = 20\ \mu m$ showing the angles between $\Delta\theta_i$ between segments. (b) Simulated worm with a 1.5 µm persistence length, a contour length of 10 µm and $\Delta s = 25\ nm$.

These simulated polymers were convolved with a two dimensional Gaussian with a full-width-at-half-maximum (FWHM) equal to the diffraction-limited point spread function of our optical system. This resulted in polymers with the same pixelation and resolution as the fluorescence images of the BTA polymers. Background Poisson noise was added to mimic the readout noise of the EMCCD together with Poisson noise to mimic shot noise. This resulted in images with comparable signal-to-noise (~10) and signal-to-background (~2.5) ratios to our experimental images.

Poissonian noise was generated using the rejection method, a technique to generate random deviates from a known and computable distribution function *p(x)dx*.[4] The rejection method requires a continuous distribution, whereas the Poisson distribution

$$Prob(j) = \int_{j-\epsilon}^{j+\epsilon} p_x(m)dm = \frac{x^j e^{-x}}{j!}, \tag{S4}$$

where *j* is the number of events occurring in an interval *x*, is discrete. This results in a distribution function that is zero everywhere, except where *m* is an integer larger or equal to zero. By defining a continuous distribution

$$q_x(m)dm = \frac{x^{[m]} e^{-x}}{[m]!} dm, \tag{S5}$$

where *[m]* is the largest integer less than *m*, the rejection method can be used. Now when a noninteger deviate is generated, it is rounded to the next lower integer part and from this deviate a random number is drawn from the Poisson distribution.

Persistence length analysis of simulated polymers

100 polymers with a 1.5 µm persistence length were simulated using the worm-like chain model. From the generated angles the apparent persistence length were calculated using cosine correlation analysis. The resulting distribution is shown in Fig. S3a and yields a persistence length of 1.50 ± 0.31 µm (median ± median absolute deviation, MAD). In order to compare simulations to experiments, polymers with the same pixelation and diffraction-limited resolution were generated by convolving the simulated polymers with a 2D Gaussian with a FWHM equal to the experimental point spread function. Persistence length analysis of convolved and pixelated polymers yielded the distribution of apparent persistence lengths shown in Fig. S3b. The resulting persistence length is 1.64 ± 0.36 µm, showing an increase in persistence length and slight broadening of the distribution. This shift and broadening both increase when shot noise is added to the images to accurately mimic the experimental images. The distribution of apparent persistence lengths yields a persistence length of 1.80 ± 0.44 µm, which means convolution and pixelation with added shot noise results in a 0.3 µm increase in persistence length compared to the persistence length of the simulated polymers, where both the convolution and pixelation and the added noise contribute equally to the increase.

In Fig. S3d and e the apparent persistence lengths of the 100 simulated polymers are correlated to the convolved and pixelated polymers (d) and the same polymers with shot noise (e). Both show excellent correlation and linear fits with a slope of 1.10 ± 0.01 (d) and 1.18 ± 0.02 (e) again reveal the increase in apparent persistence length.

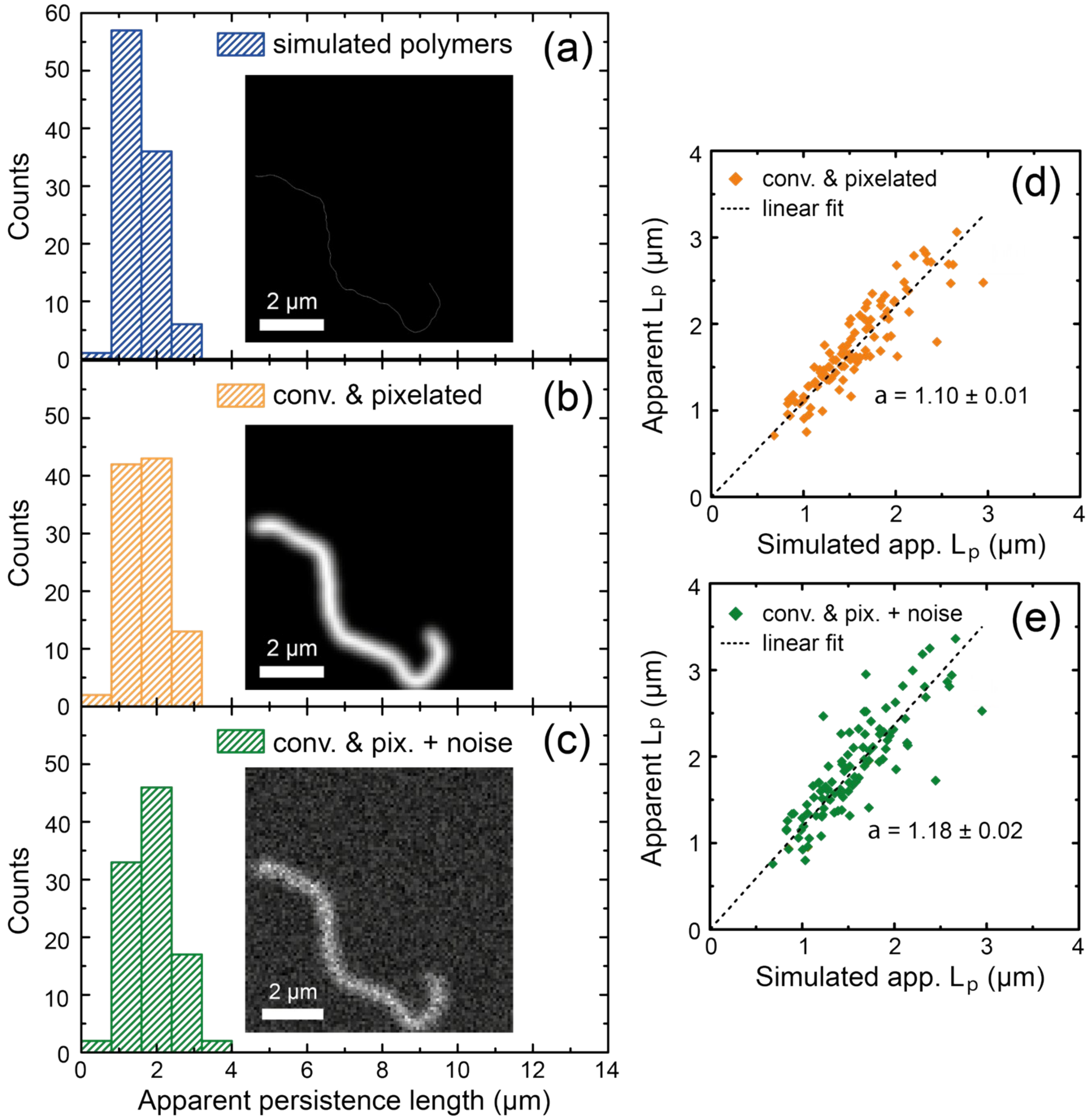

Fig. S3. Results of persistence length analysis of simulated polymers. (a) Distribution of apparent persistence lengths of simulated polymers. The apparent persistence length is directly calculated from the generated angles at the coordinate along the polymer, yielding a persistence length of 1.50 ± 0.31 µm. Inset: simulated polymer with a contour length of 10 µm and a 1.5 µm persistence length. (b) Distribution of apparent persistence lengths of pixelated simulated polymers convolved with a 2D Gaussian yields a persistence length of 1.64 ± 0.36 µm. Inset: convolved and pixelated polymer. (c) Distribution of apparent persistence lengths of convolved and pixelated polymer with added shot noise yield a persistence length of 1.80 ± 0.44 µm. Inset: convolved and pixelated polymer with added shot noise. (d) Correlation of apparent persistence lengths of 100 simulated polymers with the convolved and pixelated version of the same polymer. A linear fit yields a slope *a* of 1.10 ± 0.01. (e) Correlation of apparent persistence lengths of 100 simulated polymers with the convolved and pixelated version with added shot noise of the same polymer. A linear fit yields a slope *a* of 1.18 ± 0.02.

Immobilized BTA polymers experiencing flow

Some polymers experienced local flow, evident from the fact that multiple polymers were aligned and stretched in the same direction (Fig. S3). These were excluded from persistence length analysis by eye, where the criterion was that flow was present when two or more polymers were aligned in the same direction.

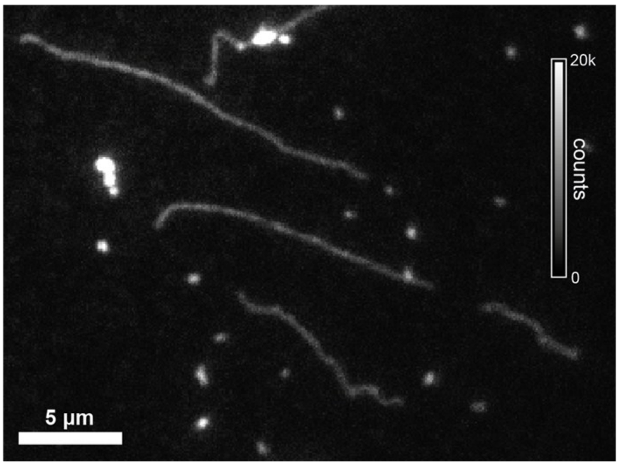

Fig. S4. Polymers experiencing flow. Local fluid flow aligns and stretches the polymers.

Analysis of AFM images of BTA polymers

The height and width of three polymers was measured from AFM images. For each polymer, the height and width is determined from Gaussian fits to cross sections along the polymer backbone. The height is defined as the amplitude of the Gaussian fit and the width as the full-width-at-half-maximum (FWHM). The polymers and distributions of the height and width determined from these polymers are shown in Fig. S5a-c. The difference in height and width between polymers depends on the polymer itself, local surface interactions, the applied force and the used AFM tip. The mean height and width as determined from these polymers varies significantly between polymers, here we measure heights of 1.3 ± 0.3 nm (a), 3.0 ± 0.4 nm (b) and 4.5 ± 0.7 nm (c) and widths of 11 ± 4 nm (a), 20 ± 6 nm (b) and 27 ± 8 nm (c), respectively. Variations in height and width are due to variations in applied force, AFM tip diameter, local differences in hydrophobicity of the surface and polymer-to-polymer variations.

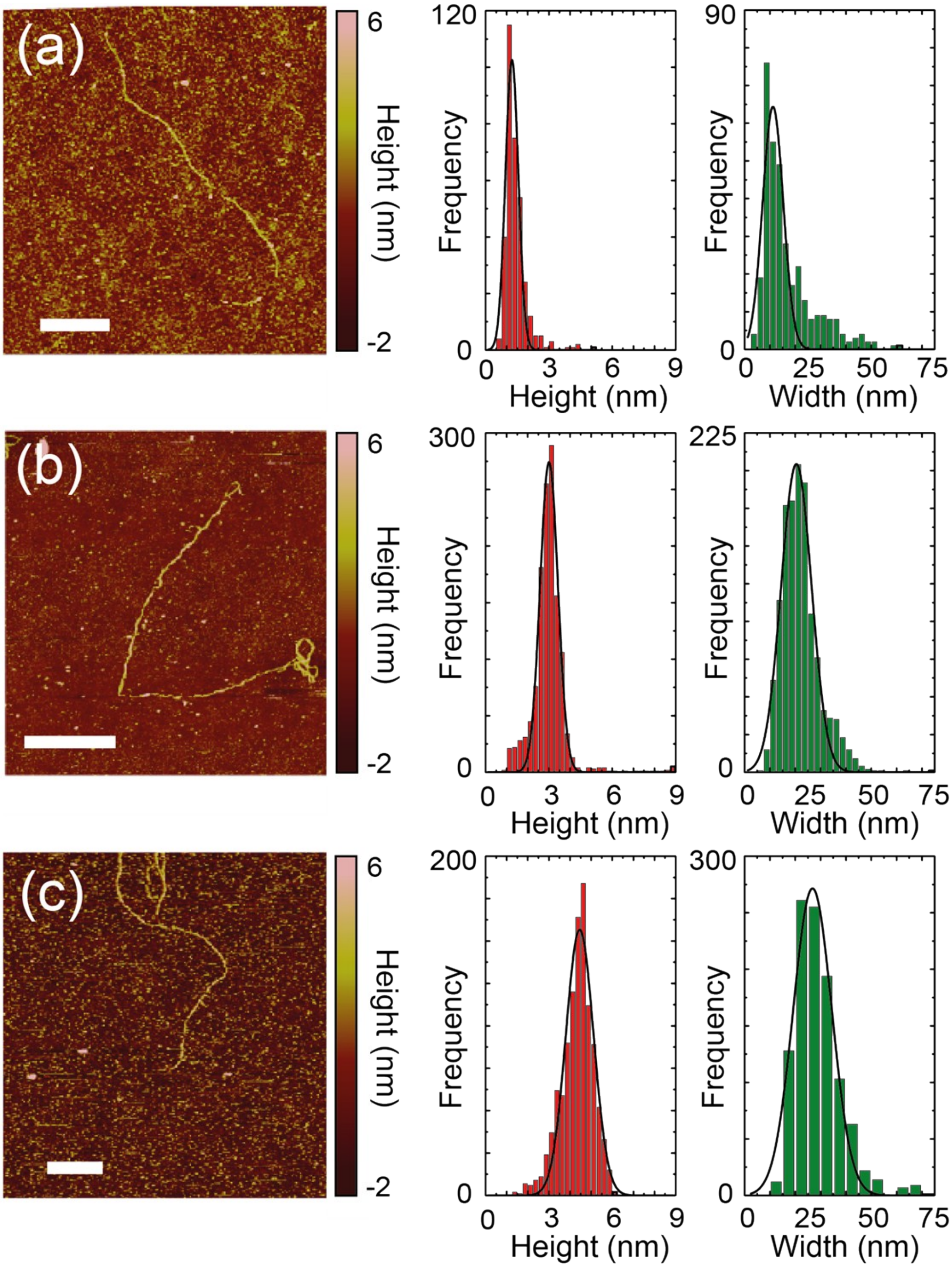

Fig. S5. Height and width analysis from AFM images. Height (red) and width (green) distributions are shown for three polymers (a-c) and were determined from Gaussian fits to cross sections along the polymer length. This yields heights of 1.3 ± 0.3 nm (a), 3.0 ± 0.4 nm (b) and 4.5 ± 0.7 nm (c) and widths of 11 ± 4 nm (a), 20 ± 6 nm (b) and 27 ± 8 nm (c). Scale bars in (a-c) are 1 µm, error bars in (d-e) are standard deviations.

To image the BTA polymers we use peak-force tapping mode, where the AFM tip (2 nm tip radius, stiffness k = 0.07 – 0.7 Nm) is modulated with a maximum force of 200 pN as feedback.

BTA polymers immobilized on a glass coverslip are fragile, although a few AFM images of mostly intact BTA polymers were recorded (see Fig. 3 in the main text and Fig. S5), the majority of BTA polymers was severely damaged due to interaction with the AFM tip. In Fig. S6 two examples are shown.

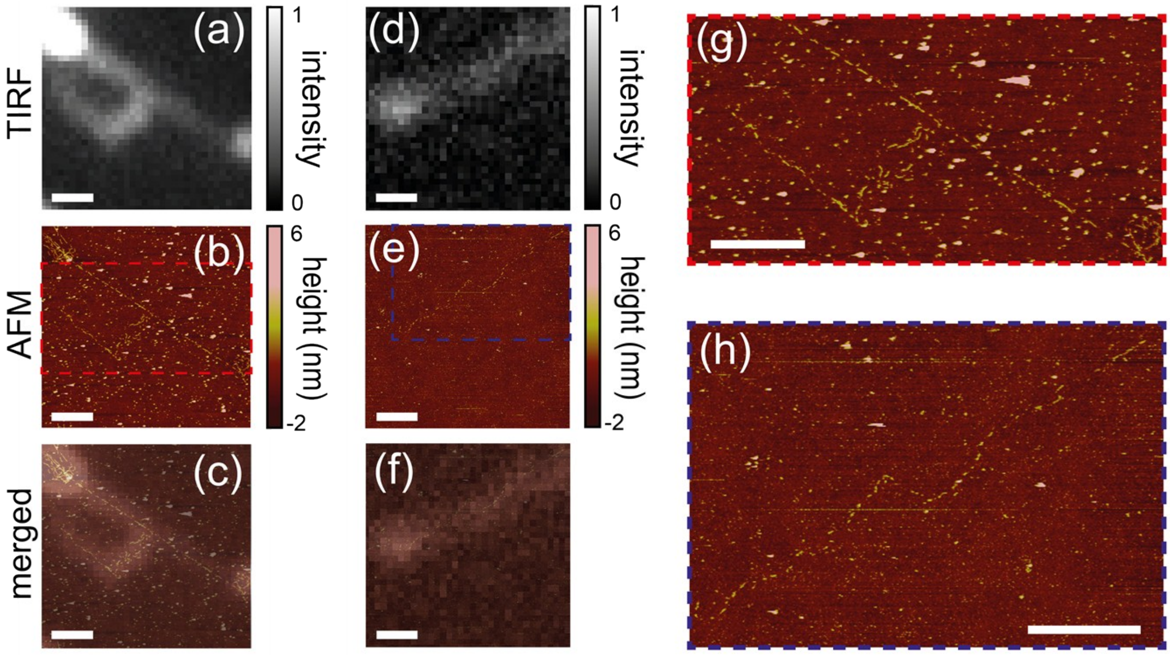

Fig. S6. Correlated AFM and TIRF images of damaged BTA polymers. TIRF (a,d), AFM topography (b,e) and merged (c,f) images of damaged BTA polymers are shown. (g) and (h) are zooms of the (b) and (e), respectively, to show the damaged polymers more clearly. All scale bars are 1 µm.

BTA polymers that remain mostly intact after the first AFM scan are damaged in subsequent scans as shown in Fig. S7a-d. Here bundling might result in more stably bound polymers compared to the single polymers in Fig. S6. Arrows indicate regions where the polymers are damaged. AFM measurements also seem to influence the polymer height in some cases as evidenced by the height and width of three regions for multiple scans. The height and width was determined by fitting a Gaussian function to a distribution of the height and width determined from Gaussian fits to cross sections along the polymer indicated by the shaded regions (1), (2) and (3). The height of the polymer decreases (Fig. S7e) for region (2) and (3), but remained constant in region (1). The width (Fig. S7f) increases in regions (2) and (3) and decreases again. For region (1) the width remains constant. This suggests AFM measurements influence the shape of the polymers, but the degree of influence varies between regions and polymer and is mostly influenced by local differences in surface interactions.

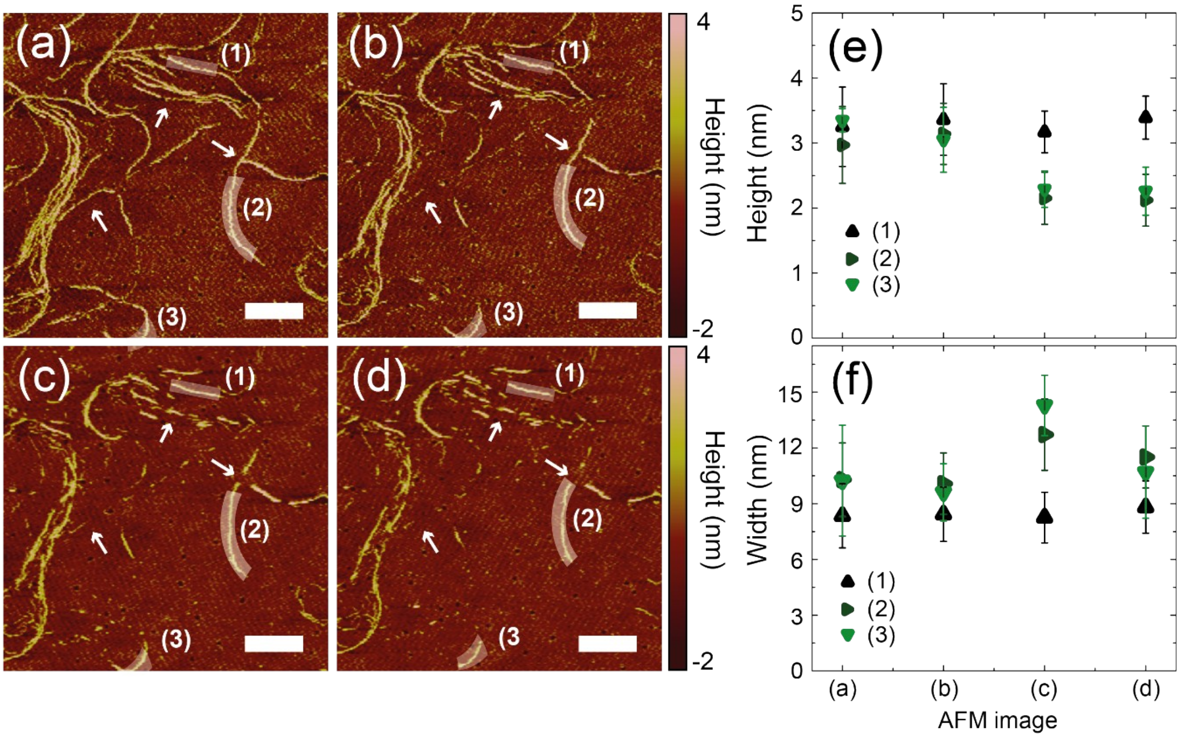

Fig. S7. Sample fragility and damage. (a-d) Four sequential AFM images of the same area showing multiple BTA polymers. Arrows indicate parts of polymers being swept away. Dashed lines indicate polymer cross sections shown in (e-g). Scale bars are 250 nm. Images were scanned with MSNL-A tips from Bruker (2 nm diameter, *k*=0.07 Nm) at 500 pN. Gaussian fit to cross sections taken from (a-d) at three different locations show a decrease in polymer height (e) and a slight increase in polymer width (f), suggesting that the AFM tip deforms the polymers.

Comparison of persistence lengths

In Fig. S8 the persistence lengths of ssDNA,[5] dsDNA,[6] actin[7] and microtubules[8] are compared to the persistence length of BTA (2.2 µm).

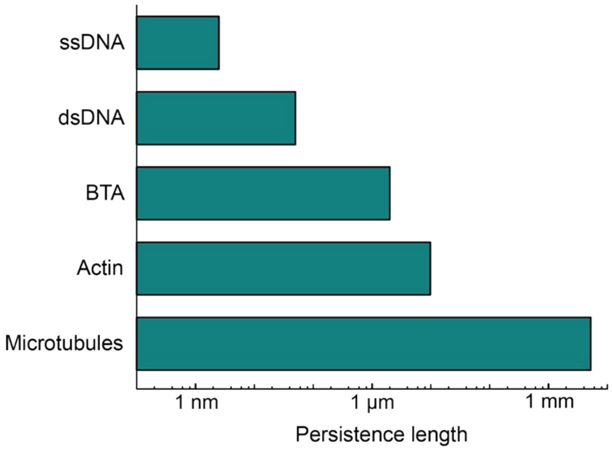

Fig. S8. Persistence lengths of different biological supramolecular polymers and BTA.

References

1. O. Kratny and G. Porod. Röntgenuntersuchung gelöster Fadenmoleküle. *Rec. Trav. Chim. Pays-Bas.*, 1949, **68**, 1106-1123.
2. C.P. Broedersz and F.C. MacKintosh. Modeling semiflexible polymer networks. *Rev. Mod. Phys.* , 2014, **86**, 995-1036.
3. J.S. Graham, B.R. McCullough, H. Kang, W.A. Elam, W. Cao and E.M. de La Cruz. Multi-platform compatible software for analysis of polymer bending mechanics. *PLoS One*, 2014, **9(4)**, e94766.
4. W.H. Press, S.A. Teukolsky, W.T. Vetterling and B.P. Flannery. *Numerical recipes in C: the art of scientific computing,* 2nd ed., Cambridge university press, New York, NY, USA, 1988.
5. M.C. Murphy, I. Rasnik, W. Cheng, T.M. Lohman and T.J. Ha. Probing single-stranded DNA conformational flexibility using fluorescence spectroscopy. *Biophys. J.*, 2004, **86**, 2530-2537.
6. P.J. Hagerman. Flexibility of DNA, *Ann. Rev. Biophys. Biophys. Chem.*, 1988, **17**, 265-86.
7. B.R. McCullough, L. Blanchoin, J-L. Mariel and E.M. de La Cruz. Cofilin increases the bending flexibility of actin filaments: implications for severing and cell mechanics. *J. Mol. Biol.*, 2008, **381**, 550-558.
8. F. Gittes, B. Mickey, J. Nettleton and J. Howard. Flexural rigidity of microtubules and actin filaments measured from thermal fluctuations in shape. *J. Cell Biol.*, 1993, 120, 923-934.